GEOPHYSICS, VOL. 84, NO. 1 (JANUARY-FEBRUARY 2019); P. MR13–MR23, 7 FIGS., 1 TABLE.
10.1190/GEO2018-0017.1

Rock-physics templates based on seismic *Q*

Stefano Picotti[1], José M. Carcione[2], and Jing Ba[3]

ABSTRACT

We build rock-physics templates (RPTs) for reservoir rocks based on seismic quality factors. In these templates, the effects of partial saturation, porosity, and permeability on the seismic properties are described by generalizing the Johnson mesoscopic-loss model to a distribution of gas-patch sizes in brine- and oil-saturated rocks. This model addresses the wave-induced fluid flow attenuation mechanism, by which part of the energy of the fast P-wave is converted into the slow P (Biot) diffusive mode. We consider patch sizes, whose probability density function is defined by a normal (Gaussian) distribution. The complex bulk modulus of the composite medium is obtained with the Voigt-Reuss-Hill average, and we show that the results are close to those obtained with the Hashin-Shtrikman average. The templates represent the seismic dissipation factor (reciprocal of seismic quality factor) as a function of the P-wave velocity, acoustic impedance, and V_P/V_S (P to S velocity ratio), for isolines of saturation, porosity, and permeability. They differentiate between oil and brine on the basis of the quality factor, with the gas-brine case showing more dissipation than the gas-oil case. We obtain sensitivity maps of the seismic properties to gas saturation and porosity for brine and oil. Unlike the gas-brine case, which shows higher sensitivity of attenuation to gas saturation, the gas-oil case shows higher sensitivity to porosity, and higher acoustic impedance and V_P/V_S sensitivity values versus saturation. The RPTs can be used for a robust sensitivity analysis, which provides insights on seismic attributes for hydrocarbon detection and reservoir delineation. The templates are also relevant for studies related to CO_2-storage monitoring.

INTRODUCTION

Rock-physics templates (RPTs) link the elastic properties (e.g., velocity, density, seismic impedance, wet-rock stiffness moduli, and seismic dissipation factor) and reservoir properties such as porosity, fluid saturation, permeability, and lithology (e.g., Avseth et al., 2005; Carcione and Avseth, 2015). Seismic attenuation has been scarcely used to build templates, despite the fact that the quality factor is very sensitive to saturation and permeability. In fact, when seismic waves propagate through small-scale heterogeneities, pressure gradients are induced between regions of dissimilar elastic properties. White (1975) and Johnson (2001) — who considered spherical gas pockets and gas patches of arbitrary shape, respectively — showed that seismic attenuation and velocity dispersion measurements can be explained by the effect of mesoscopic-scale inhomogeneities and energy transfer between wave modes combined with P-wave to slow P (Biot)-mode conversion. We refer to this mechanism as mesoscopic loss. The mesoscopic-scale length is intended to be much larger than the grain sizes but much smaller than the wavelength of the seismic pulse. For instance, if the type of saturating pore fluid varies significantly from point to point, diffusion of pore fluid between different regions constitutes a mechanism that can highly affect attenuation at seismic frequencies (a range between 5 and 200 Hz). Reviews of different models to understand this mechanism can be found, for instance, in Carcione and Picotti (2006), Müller et al. (2010), and Carcione (2014).

We build RPTs addressing the P-wave seismic attenuation caused by partial saturation of gas. The first to attack this problem were Dvorkin and Mavko (2006), who discriminate gas sandstone from wet sandstone. Here, we describe the effects of varying partial saturation, porosity, and permeability by a generalization of the Johnson mesoscopic-loss model to the case of patches of different

Manuscript received by the Editor 18 January 2018; revised manuscript received 12 August 2018; published ahead of production 25 September 2018; published online 23 November 2018.
Istituto Nazionale di Oceanografia e di Geofisica Sperimentale (OGS), Borgo Grotta Gigante 42c, 34010 Sgonico, Trieste, Italy.
[2]Istituto Nazionale di Oceanografia e di Geofisica Sperimentale (OGS), Borgo Grotta Gigante 42c, 34010 Sgonico, Trieste, Italy and Hohai University, School of Earth Science and Engineering, Nanjing, 211100, China.
[3]Hohai University, School of Earth Science and Engineering, Nanjing, 211100, China. E-mail: jba@hhu.edu.cn.

sizes. We vary the radius of the patches (White model) according to a probability density function (PDF) of a normal distribution. Generalizing the White model to the Johnson model is achieved by increasing the surface-to-volume ratio parameter for spherical patches, (S/V in Johnson, 2001), describing rough gas-brine interfaces.

We consider specific relations to obtain the dry-rock moduli and the permeability, namely, the Krief and Kozeny-Carman equations, respectively, but in practice, the model has to be calibrated with log and seismic data to obtain these properties. Alternative models describing attenuation and velocity dispersion in fractal media have been developed by Toms et al. (2007) and Müller et al. (2008), assuming a multiple-scattering approach to approximate the scattered field of a system of randomly distributed poroelastic inclusions.

Sensitivity analysis can identify the rock properties exerting the dominant impact on the seismic attributes (Hamby, 1994). Identification of these petrophysical properties is useful for evaluating the effectiveness of certain seismic attributes in hydrocarbon exploration and CO_2 monitoring. In this process of evaluating effectiveness, rock-physics models are used to assess which seismic attribute is more sensitive to detect the presence of gas or to reliably estimate the spatial extent of a reservoir. In CO_2-storage monitoring, seismic attributes sensitive to the presence of gas can also detect CO_2 leakages in the overlying formations (Picotti et al., 2012). However, sensitivity analysis of seismic attributes often involves complex numerical procedures, such as the calculation of synthetic seismograms, which is computationally demanding. In fact, the simulation of synthetic seismograms requires solving Biot's differential equations on a very fine computational grid to capture the loss mechanism of converting fast P-wave energy to diffusion energy in the form of the Biot slow wave. A computationally efficient approach is to approximate White's moduli by the Zener model (e.g., Carcione et al., 2012; Picotti et al., 2010) or the Cole-Cole model (Picotti and Carcione 2017) and then solve the single-phase viscoelastic differential equations.

In summary, the state of the art indicates that RPTs based on attenuation were only studied by Dvorkin and Mavko (2006). Here, we extend their work to a detailed analysis involving different fluids and seismic and transport properties, such as varying porosity, saturation, and permeability. Our approach is based on a generalization of the Johnson theory of mesoscopic attenuation. We show that the use of RPTs allows for a faster, and at the same time more reliable, sensitivity study than full-wave inversion methods.

METHODOLOGY

In this section, we introduce the models for building the RPTs. Specifically, we describe the rock basic properties, such as permeability, dry-rock moduli, fluid properties, the model to obtain the effective wet-rock modulus, the seismic-wave characteristics (phase velocity and quality factor), and the sensitivity-analysis method.

Matrix and fluid properties

In the Kozeny-Carman relationship (Carman, 1961), permeability κ is related to porosity ϕ through:

$$\kappa = \frac{\kappa_0 \phi^3}{(1-\phi)^2}, \tag{1}$$

here, we assume a realistic value of $\kappa_0 = 2.5$ D. For example, if $\phi = 1/3$, we have $\kappa = \kappa_0/12 = 0.2$ D, a typical value for clastic reservoir rocks. Equation 1 is a classical model for the permeability of porous media, which is a sufficient approximation. However, other expressions can perform better provided that a proper calibration is performed. Another possibility is to use mineral composition. Herron (1987) used explicit mineralogical information available from geochemistry to obtain estimates of porosity and permeability. He quantified the effects of the minerals composing the rock by defining specific weights. In any case, the Kozeny-Carman equation is the most used because it is based on physical principles (e.g., Tiab and Donaldson, 2015).

We use Krief model (Krief et al., 1990) to obtain the dry-rock moduli K_m and $\mu_m \equiv \mu$. The moduli are given by

$$\begin{aligned} K_m &= K_s(1-\phi)^{4/(1-\phi)}, \\ \mu &= K_m \mu_s / K_s, \end{aligned} \tag{2}$$

where K_s and μ_s are the bulk and shear moduli of the solid grains, respectively. The porosity dependence in equation 2 is consistent with the concept of critical porosity because the moduli should be small above a certain porosity value (usually from 0.4 to 0.6).

The mesoscopic-loss effect is enhanced when the two fluids are quite different, such as gas and brine. The properties of the fluids depend on temperature and pressure, which can directly correlate to depth z. The gas adiabatic bulk modulus and density can be calculated from the Peng-Robinson equation of state, whereas the properties of brine are given by the Batzle and Wang relations. Picotti et al. (2012) use this approach to obtain the fluid properties.

Mesoscopic-loss model with varying patch sizes: effective wet-rock modulus

The seismic properties are determined from a mesoscopic rock-physics theory (Johnson, 2001) for robust estimation of attenuation as a function of porosity, gas saturation, fluid viscosity, and permeability (see Appendix A). It is assumed that the medium has gas patches of mesoscopic size in a uniform background, where mesoscopic means smaller than the wavelength and larger than the pore size, e.g., centimeters compared with tens of meters and micrometers, respectively.

Johnson (2001) describes wave velocity and attenuation as a function of frequency for the given surface-to-sample-volume ratio $\beta = S/V$ of the mesoscopic patches. This parameter defines the shape of the patch, as it is illustrated in Appendix A for an ellipsoidal geometry. A second parameter of the model T describes the size of the patch. Johnson generalized the White model (White, 1975) for spherical patches. White developed a model for a gas-filled sphere of porous medium of radius a located inside a water-filled cube of porous medium. To further simplify the calculations, White considers an outer sphere of radius b (i.e., $b > a$), instead of a cube, where $S_g = a^3/b^3$. At the same time, $\beta = 3S_g/a$, where S_g is the gas saturation (see equation A-25). We consider this value of β as a lower limit, whereas the parameter T in the Johnson theory is assumed to be that of White (see Appendix A).

Having the single wet-rock complex moduli corresponding to each patch size, the complex bulk modulus of the composite medium is obtained with the Voigt-Reuss-Hill (VRH) average. This average is based on isostrain (Voigt) and isostress (Reuss) approximations (the stress and strain are unknown and are expected to be nonuniform). The VRH estimates were found in most cases to have an accuracy comparable to that of the self-consistent schemes and

are valid for complex rheologies such as anisotropy (e.g., Man and Huang, 2011).

We generalize the Johnson theory to the case of a distribution of patch radii $a_j, j = 1, \ldots, J$, based on a normal PDF. The normal distribution from $a_0 - \Delta a$ to $a_0 + \Delta a$ is given by the Gaussian function

$$\mathrm{PDF}_j = \frac{\delta}{\sqrt{2\pi\sigma}} \exp[-(a_j - a_0)^2/(2\sigma^2)], \tag{3}$$

where a_0 is the dominant radius and σ is the variance of the distribution. There are J radii equispaced at an interval $\delta = 2\Delta a/(J-1)$. Other PDFs can be found in Engelsen et al. (2002).

We obtain J complex moduli K_j describing the anelastic properties of each porous medium with radius a_j (see equation A-12) by the VRH average. The Voigt (K_V) and Reuss (K_R) averages are isostrain and isostress approximations, respectively (the stress and strain are unknown and are expected to be nonuniform). The VRH is close in accuracy to more sophisticated techniques such as self-consistent schemes and are applicable to complex rheologies such as general anisotropy and arbitrary grain topologies (e.g., Man and Huang, 2011). We calculate the effective bulk modulus as

$$K = \frac{1}{2}(K_V + K_R), \tag{4}$$

where

$$K_V = \sum_j \mathrm{PDF}_j K_j \quad \text{and} \quad K_R^{-1} = \sum_j \mathrm{PDF}_j K_j^{-1} \tag{5}$$

An alternative method is to assume that the effective bulk modulus is equal to the arithmetic average of the upper and lower Hashin-Shtrikman (HS) bounds (Hashin and Shtrikman, 1963; Carcione et al., 2006; Mavko et al., 2009). The shear modulus is not affected by the mesoscopic loss. In subsequent sections, we show that the heuristic VRH average is approximately equal to the HS average for the problem at hand.

The effective density is given by the arithmetic average:

$$\rho = \sum_j \mathrm{PDF}_j \rho_j. \tag{6}$$

For a given patch radius a, the location of the White relaxation peak is

$$f_p = \frac{\kappa_b K_{E_b}}{\pi\eta_b (b-a)^2} = \frac{\kappa_b K_{E_b}}{\pi\eta_b a^2 (S_g^{1/3} - 1)^2} \tag{7}$$

(White, 1975; Carcione, 2014, equation 7.449), where the subindices "g" and "b" stand for gas and brine, respectively. Increasing a implies decreasing the peak frequency. In general, mesoscopic models of attenuation give a relaxation peak whose peak frequency (maximum attenuation) obeys

$$f_p \propto \frac{\kappa_b}{\eta_b a^2} \tag{8}$$

Therefore increasing the size of the patch and fluid viscosity implies a lower peak frequency, whereas increasing the permeability implies a higher peak frequency.

Phase velocity and quality factor

The complex velocity is the key parameter to quantify the phase velocity and seismic quality factor. The complex P-wave velocity is predicted by the Johnson model as

$$v_c(\omega) = \sqrt{\frac{K(\omega) + 4\mu/3}{\rho}} \tag{9}$$

where μ is the dry-rock shear modulus, and ω is the angular frequency. The bulk density is given by equation 6, which reduces to

$$\rho = (1-\phi)\rho_s + \phi\rho_f, \tag{10}$$

where ρ_s and ρ_f are, respectively, the effective densities of the mineral matrix and the pore fluid and ϕ is the porosity. The effective density of the pore fluid is

$$\rho_f = S_g\rho_g + S_b\rho_b, S_b = 1 - S_g, \tag{11}$$

where S_b and S_g are the brine and gas saturations, respectively. According to some studies such as Carcione (2014), the P-wave phase velocity and seismic quality factor are

$$v = \left[\mathrm{Re}\left(\frac{1}{v_c}\right)\right]^{-1} \tag{12}$$

and

$$Q = \frac{\mathrm{Re}(v_c^2)}{\mathrm{Im}(v_c^2)}. \tag{13}$$

Sensitivity analysis

RPTs are useful to construct sensitivity maps related to key seismic properties, such as the P-wave dissipation factor and velocity, acoustic impedance, and V_P/V_S ratio. Combining synthetic seismograms with the appropriate rock-physics models, Böhm et al. (2015) show that petrophysical properties of a medium (e.g., porosity and gas saturation) can be derived from velocity and quality factor maps, determined from attenuation and traveltime tomography. In contrast, the most significant seismic-loss mechanisms in hydrocarbon reservoirs are a result of porosity variations and partial saturation, where one of the fluids is significantly stiffer than the other (e.g. Carcione and Picotti, 2006). Therefore, the estimation of the sensitivity of the key seismic properties versus porosity and gas saturation can be insightful in hydrocarbon seismic exploration.

The approach is the following. Let $y = f(x_1, x_2)$ be the relation between a dependent variable y and two independent variables x_1, x_2. The sensitivity function χ_i versus x_i $(i = 1, 2)$ can be defined as

$$\chi_i = \frac{x_i}{f(x_1, x_2)} \frac{\partial f(x_1, x_2)}{\partial x_i}, \quad i = 1, 2 \tag{14}$$

(Hamby, 1994), where the quotient $x_i/f(x_1, x_2)$ is introduced to normalize the function by removing the effects of the units. In our case, the dependent variable y can be either the dissipation factor, the P-wave velocity, the acoustic impedance, or the phase velocity ratio V_P/V_S, whereas the dependent variable x_i can be either the porosity $(i = 1)$ or the gas saturation $(i = 2)$. It follows that the sensitivity

versus porosity (or saturation) is not a simple coefficient but a function of the two independent variables.

ROCK-PHYSICS TEMPLATES AND RESULTS

As stated previously, Johnson mesoscopic model of patchy saturation is used to describe the attenuation and the velocity dispersion of the seismic waves (see Appendix A). The surface-to-sample-volume ratio β, a free parameter describing the shape of the patch, is assumed to be given by

$$\beta = \frac{3S_g\zeta}{a}, \zeta \geq 1, \tag{15}$$

where ζ is a dimensionless parameter, with $\zeta = 1$ giving the White model. The fact that ζ is greater than one implies that the gas-brine contact is rough and that the shape of the patch is not spherical. An example of a 3D ellipsoidal patch is illustrated in Appendix A, where β is given by equation A-20.

We consider the material and fluid properties given in Table 1. The grain properties in this case are those of quartz (i.e., clean sandstone), but a mix of quartz and clay can be applied for a different lithology. Figure 1a and 1b shows the P-wave velocity, whereas Figure 1c and 1d shows the dissipation factor (reciprocal of Q) (c and d) as functions of frequency for the White and Johnson models, where $\phi = 0.35$, $S_g = 0.1$, and $\zeta = 10$. The gas-brine

Table 1. Elastic properties.

Medium	K (GPa)	μ (GPa)	ρ (g/cm3)	η (Pa s)
Grain	39	40	2.65	—
Brine	2.25	0	1.03	0.0012
Oil	2.16	0	0.8	0.24
CH_4	0.016	0	0.1	0.00001

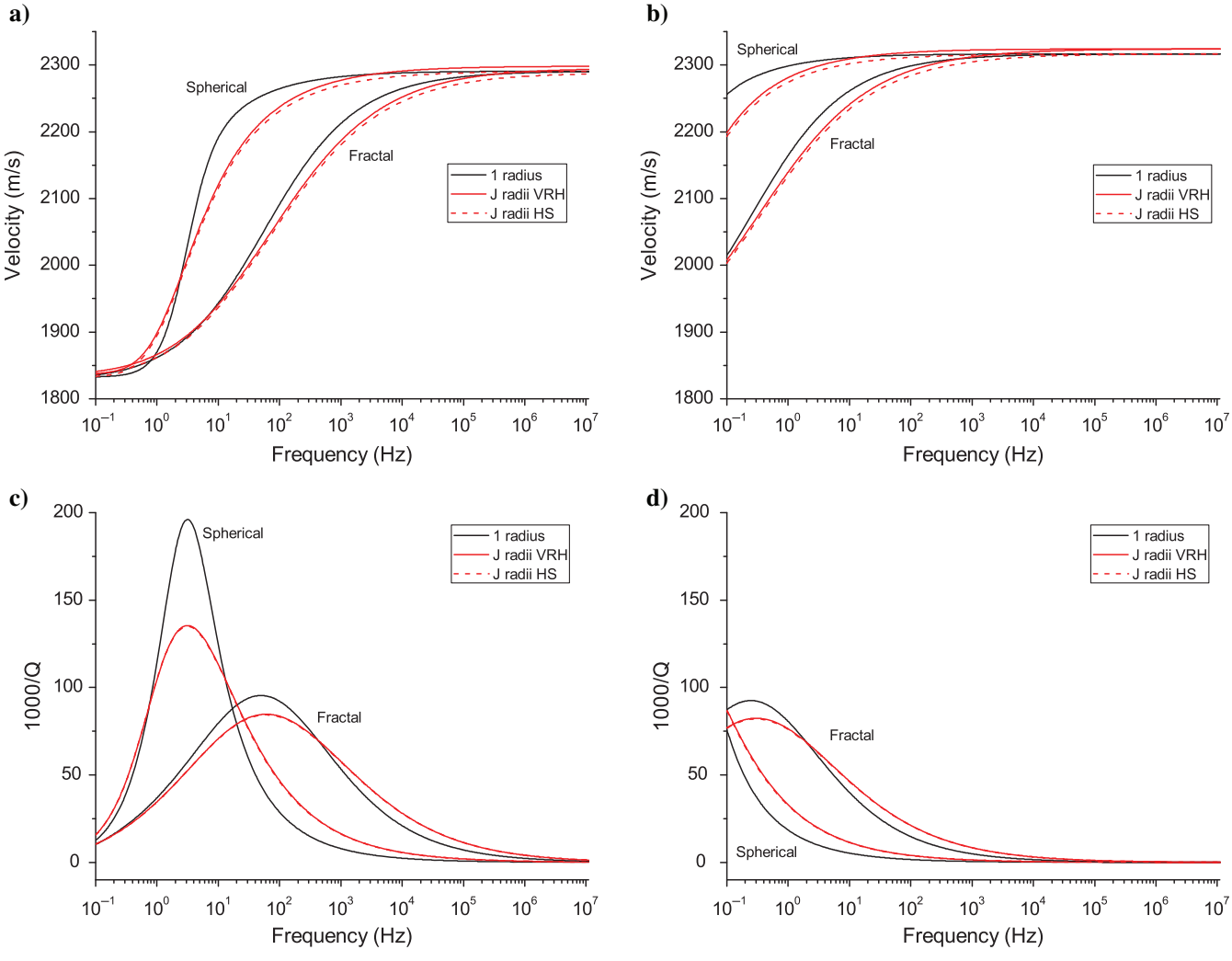

Figure 1. Phase velocity (a and b) and dissipation factor (c and d) as a function of frequency for the White (spherical geometry) and Johnson (rough geometry) models. The gas-brine (a and c) and gas-oil (b and d) cases are considered, where the mean radius a_0 is 30 cm. The results obtained by using the VRH average (solid lines) and the Hashin-Shtrikman bound average (dashed lines) are displayed. The curves for a single patch radius (black curves) are also shown.

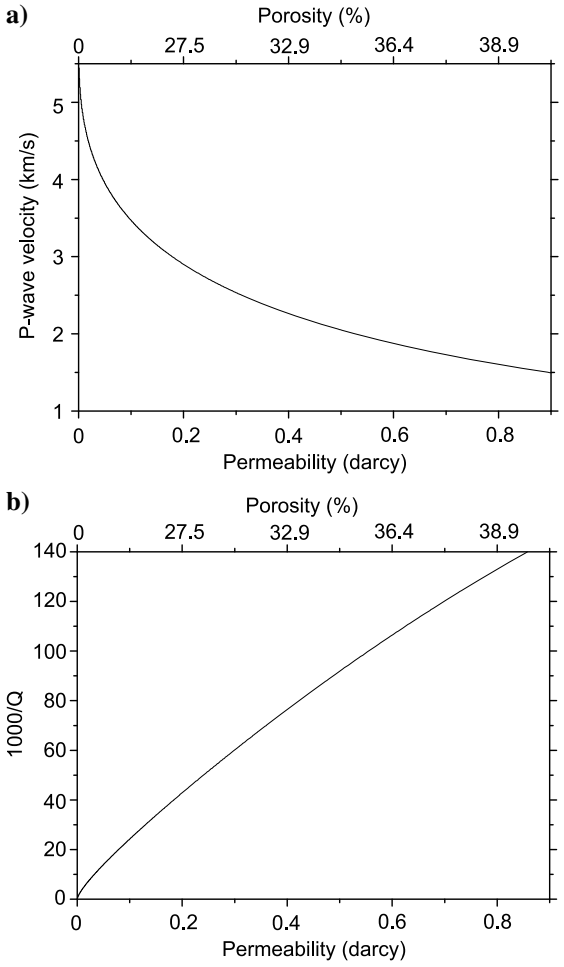

Figure 2. The P-wave phase velocity (a) and dissipation factor (b) as functions permeability and porosity for the gas-brine case. The model is that of Johnson with a distribution of radii.

(Figure 1a–1c) and gas-oil (Figure 1b–1d) cases are considered, with the mean radius $a_0 = 30$ cm, $\Delta a = 30$ cm, and $\sigma = 20$ cm in both cases. In the same figure, the same models are shown for a constant radius equal to the mean radius. As can be observed, the difference between one radius and J radii is less pronounced for the Johnson model. This difference is more evident for the dissipation factor than for the phase velocity. Moreover, the relaxation peak is located at lower frequencies for oil because of its higher viscosity than brine. The results corresponding to the VRH average (solid lines) and the HS bounds average (dashed lines) are displayed, showing that the difference between these two approaches is almost negligible at all frequencies.

In the following, the effective bulk modulus is given by the VRH average, and the frequency is assumed to be $f = 50$ Hz, a typical value in the seismic exploration band. The liquid in the pore space is brine, unless specified otherwise. The P-wave phase velocity and dissipation factor are represented in Figure 2 as functions of permeability and porosity (the model is that of Johnson with a Gaussian PDF). As the permeability increases with increasing porosity, the phase velocity decreases and attenuation increases, such that $Q = 11$ at 0.5 D.

The templates are built using $Q^{-1} = Q_P^{-1}$, without considering Q_S, since the shear waves are in principle not affected by the fluids. Figures 3, 4, and 5 show the cases for gas in brine (a) and oil (b), where the dissipation factor is represented as a function of the P-wave velocity, the acoustic impedance, and the V_P/V_S ratio, respectively. We assume a mean radius $a_0 = 30$ cm and $\zeta = 10$. The curves correspond to isolines of constant saturation and constant porosity (i.e, constant permeability). In Figure 5, the S-wave velocity is given by $v_S = \sqrt{\mu/\rho}$. For the gas-brine case, the P-wave velocity, acoustic impedance, and quality factor decrease with increasing porosity at a fixed gas saturation (black curves), but they increase or decrease in response to a variable gas saturation at a fixed porosity (red curves). The V_P/V_S increases and quality factor decreases with increasing porosity at a fixed gas saturation (black curves), but they increase or decrease as a function of gas saturation at a fixed porosity (red curves). The gas-oil case exhibits similar trends to those observed in the gas-brine case. However, the

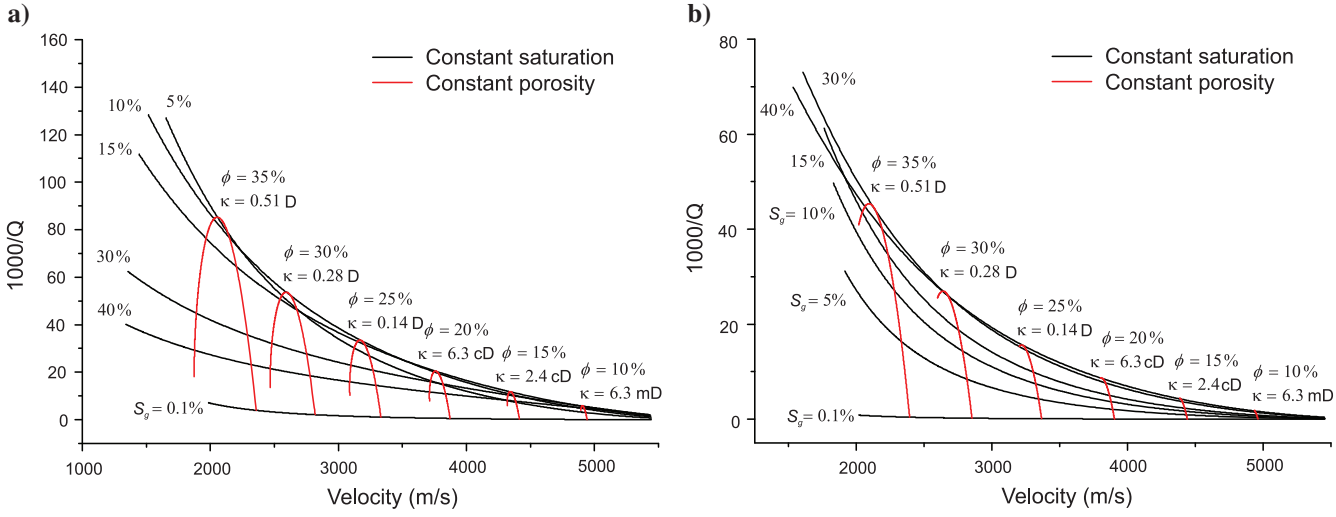

Figure 3. Rock-physics templates for gas-brine (a) and gas-oil (b). The dissipation factor is represented as a function of the P-wave velocity, including isolines of gas saturation and porosity (permeability). The rock-physics model is that of Johnson model with a distribution of radii.

dissipation factor reaches lower values by about an order of magnitude compared to the brine-gas case. This effect is particularly evident in Figure 5.

We have considered specific relations to obtain the dry-rock moduli and the permeability, namely, the Krief and Kozeny-Carman equations, respectively. However, building a template requires calibration of the model with seismic or well-log data. It is not common to calibrate a RPT to seismic and well-log data simultaneously because seismic data and well-log data have vast differences in terms of scale. There are several steps to calibrate and use the templates: (1) Obtain the effective properties of the grain minerals and pore-infill material, (2) determine the properties of the dry rock, (3) obtain the wet-rock velocities, mass density, and attenuation with a suitable model (Johnson model is used here), (4) perform pore-infill substitution to determine the location of each specific pore-infill component in the RPT, and (5) report the seismic properties on the templates to create fluid saturation maps of the studied area, through saturation isolines, as well as porosity and permeability isolines. There is obviously a scaling issue when doing this step. There also could be multiple scenarios of gas saturation and permeability/porosity that satisfy a particular spatial distribution of seismic properties/attributes such as V_P and Q.

Figures 6 and 7 show the sensitivity maps for the gas-brine and gas-oil cases, respectively. The results indicate that, in both cases, the P-wave dissipation factor is the most sensitive property. Considering the maximum sensitivity values, all the seismic properties

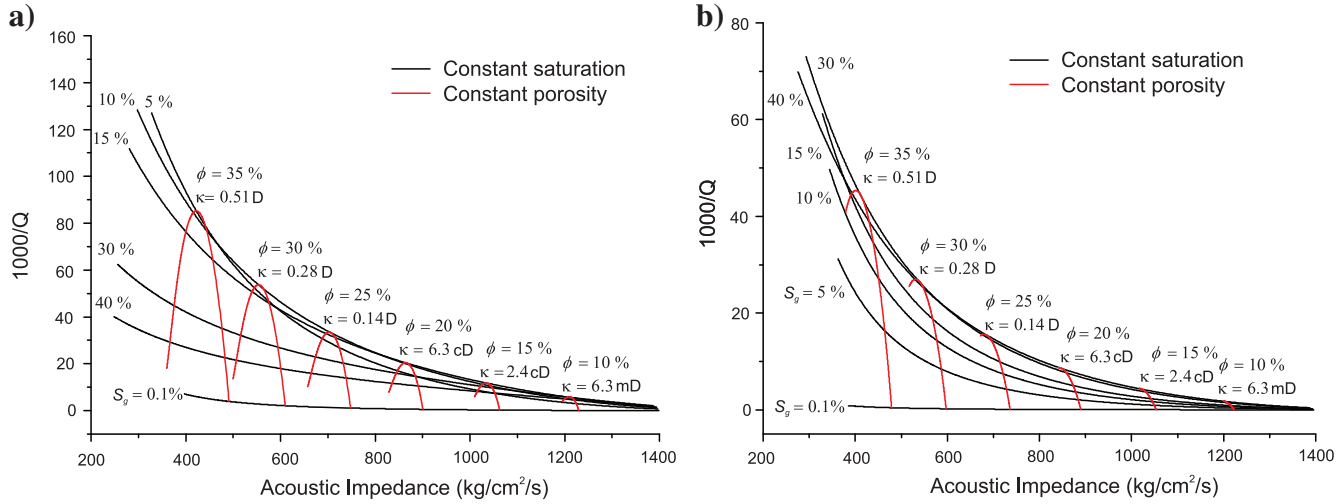

Figure 4. Rock-physics templates for gas-brine (a) and gas-oil (b). The dissipation factor is represented as a function of the acoustic impedance, including isolines of gas saturation and porosity (permeability). The rock-physics model is that of Johnson model with a distribution of radii.

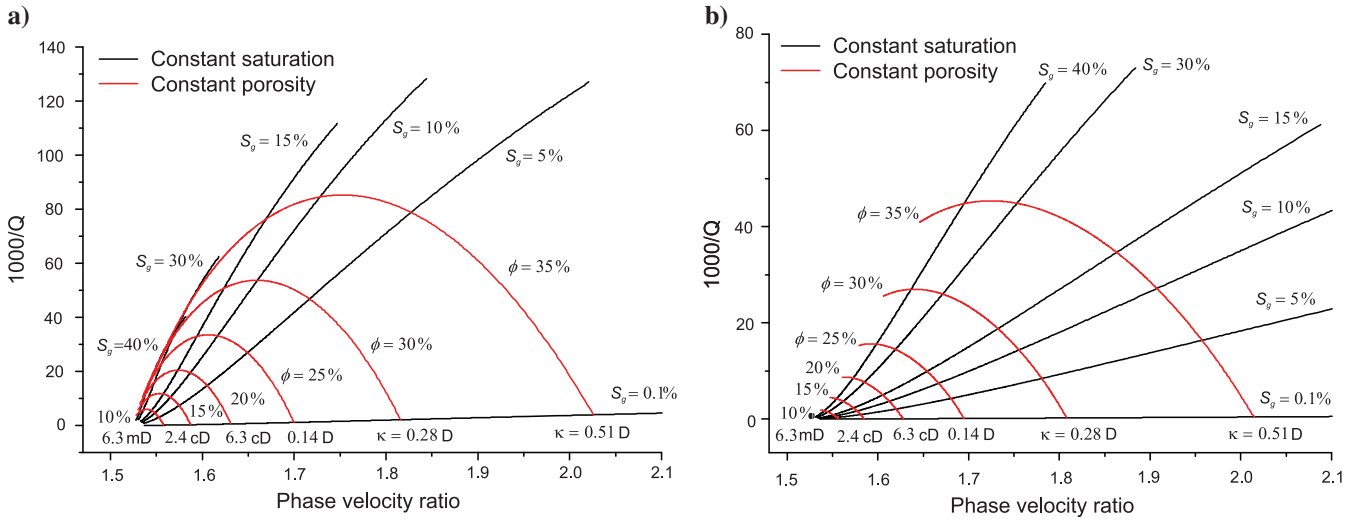

Figure 5. Rock-physics templates for gas-brine (a) and gas-oil (b). The dissipation factor is represented as a function of the V_P/V_S ratio, including isolines of gas saturation and porosity (permeability). The rock-physics model is that of Johnson model with a distribution of radii.

are more sensitive to porosity than to saturation. Generally, the sensitivity increases with increasing porosity, except for the dissipation factor sensitivity versus saturation, which exhibits complex behavior. The dissipation factor and V_P/V_S ratio sensitivity versus porosity increases with the decreasing gas saturation and increasing porosity. The sensitivity to porosity maps of all the properties are similar in the two cases. The maximum sensitivity values are similar as well, except for the dissipation factor, which exhibits a higher value for the gas-oil case. In contrast, the sensitivity to gas saturation maps is quite dissimilar. These maps indicate a higher sensitivity of the dissipation factor at high saturations and medium-high porosities for the gas-brine case, whereas it is more sensitive at low saturations or low porosities for the gas-oil case. Moreover, the P-wave velocity, acoustic impedance, and V_P/V_S ratio sensitivity exhibit a maximum at approximately 10% gas saturation in the gas-brine case, and more than 40% gas saturation in the gas-oil case. The dissipation factor is more sensitive in the gas-brine case, while the acoustic impedance and the V_P/V_S ratio show higher values for the gas-oil case. The other parameters show similar values.

When dealing with real data, the problem can be to determine the size distribution of the gas patches. Well-log data, such as the sonic velocity and the electrical resistivity profile, can provide this information. Another uncertainty is the permeability, which can be based on a calibrated Kozeny-Carman equation or on a fully empirical formula as a function of porosity. For the calibration, knowledge of the porosity (from the density and/or sonic logs) and clay content (from gamma-ray logs) is essential. Moreover, another requirement, to support the interpretation and the calibration, is laboratory experiments on core samples to obtain the porosity, grain size, tortuosity, mineral composition, and permeability.

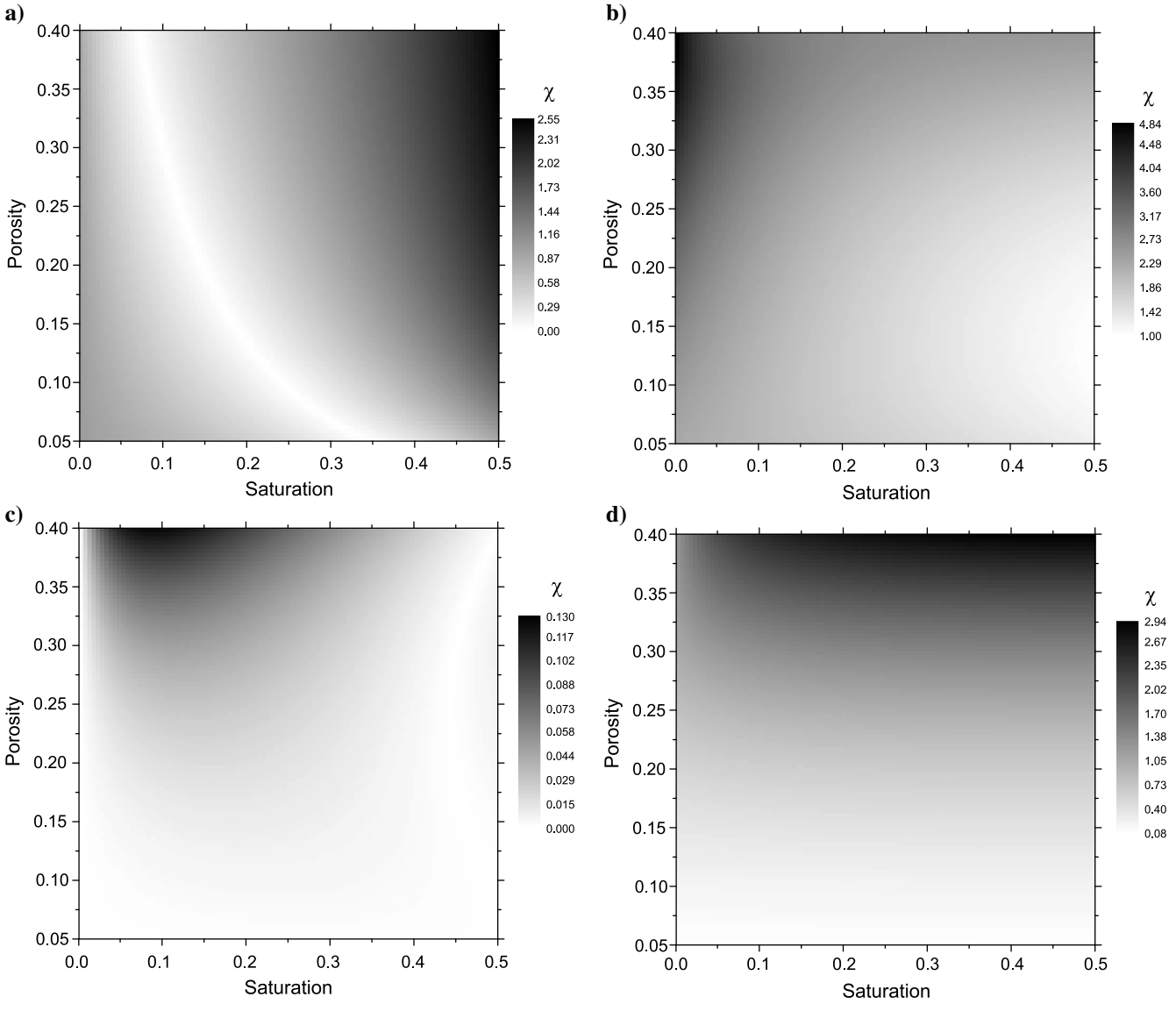

Figure 6. Sensitivity maps for the gas-brine case by using the Johnson model with a PDF: (a) dissipation factor sensitivity versus gas saturation, (b) dissipation factor sensitivity versus porosity, (c) P-wave velocity sensitivity versus gas saturation, and (d) P-wave velocity sensitivity versus porosity.

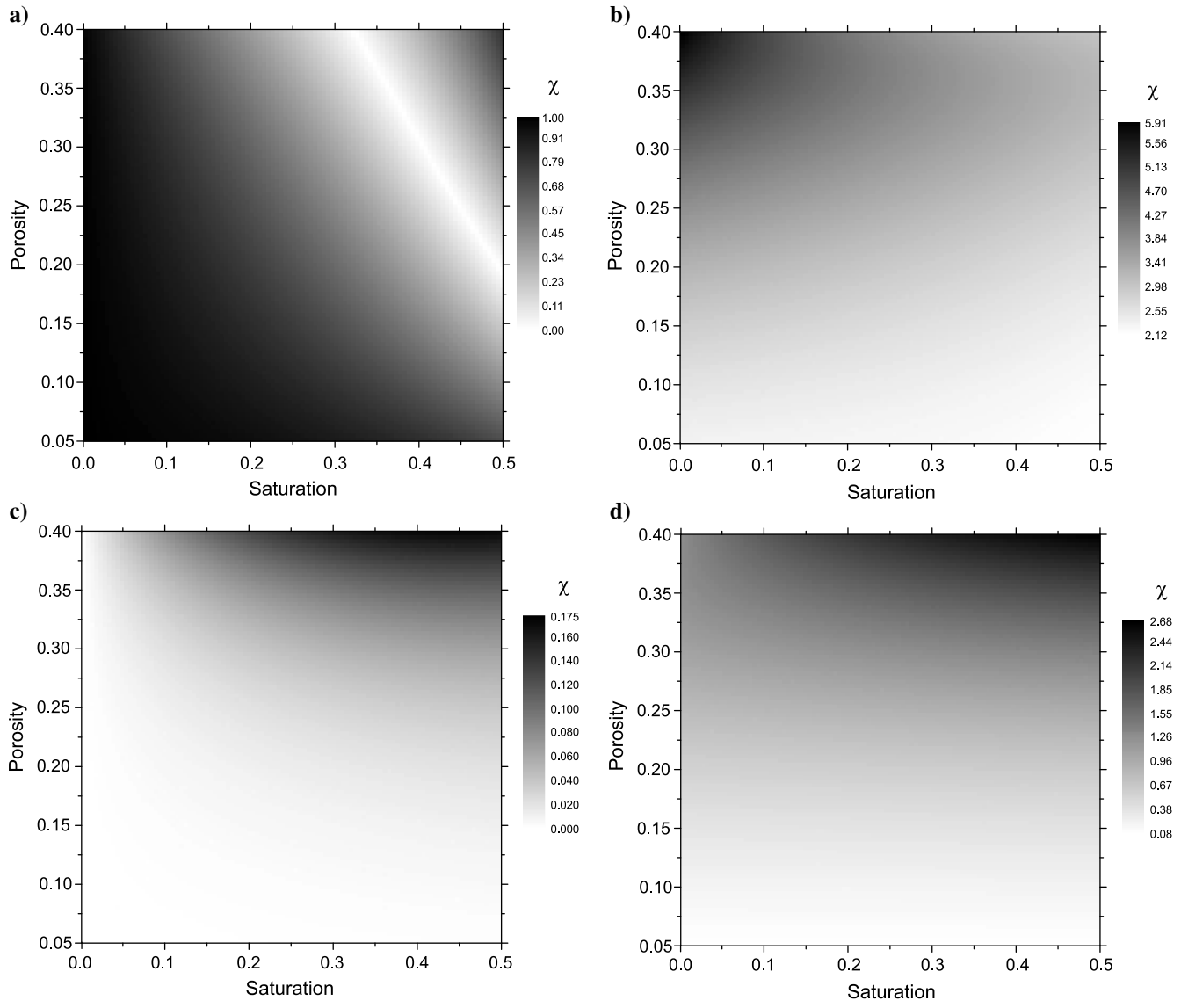

Figure 7. Sensitivity maps for the gas-oil case by using the Johnson model with a PDF: (a) dissipation factor sensitivity versus gas saturation, (b) dissipation factor sensitivity versus porosity, (c) P-wave velocity sensitivity versus gas saturation, and (d) P-wave velocity sensitivity versus porosity.

CONCLUSION

We propose a methodology to build RPTs for clastic rocks based on seismic attenuation of P-waves in partially saturated media. The loss/dispersion model is given by the Johnson mesoscopic theory generalized to the case of varying patch sizes on the basis of a Gaussian PDF. We consider a clean sandstone, but the rock-physics model can be extended to more heterogeneous lithologies, such as shaley sandstones, where the clay content affects the seismic attributes as it is the case of fluids. The mesoscopic-loss theory can be based on a composite three-phase Biot-type theory or the White theory for periodic layering because in this case, a heterogeneous matrix can be modeled in addition to different pore fluids. Moreover, other permeability laws and modulus average can be implemented depending on the specific lithology.

The templates represent the seismic dissipation factor (reciprocal of Q) versus P-wave velocity, acoustic impedance and V_P/V_S ratio, for isolines of saturation, porosity, and permeability. Two different cases are considered, where the liquid is brine or oil. In both cases, the P-wave velocity, acoustic impedance, and quality factor decrease with increasing porosity at a fixed gas saturation, while the V_P/V_S ratio increases. However, these properties may increase or decrease as a function of gas saturation at a given porosity. The dissipation factor shows higher values for brine.

Sensitivity maps of the P-wave dissipation factor, P-wave velocity, acoustic impedance, and V_P/V_S ratio versus gas saturation and porosity are also derived from the templates. The main result is that all the seismic properties are more sensitive respect to porosity than to saturation, being the dissipation factor the most sensitive. Then, while the sensitivity maps of the properties versus porosity are very similar for brine and oil, the sensitivity maps versus saturation are quite dissimilar. The gas-oil case is characterized by higher attenuation sensitivity values versus porosity, and higher acoustic impedance and V_P/V_S sensitivity values versus saturation. Moreover, the gas-brine case

shows higher dissipation factor sensitivity values versus saturation. These maps can be very useful for a fast and reliable evaluation of the effectiveness of the seismic method in hydrocarbon exploration.

ACKNOWLEDGEMENTS

We thank editor Jeffrey Shragge and two anonymous reviewers for very useful comments. This work is supported by the Specially-Appointed Professor Program of Jiangsu Province, China, and the Cultivation Program of "111" Plan of China (BC2018019).

DATA AND MATERIALS AVAILABILITY

Data associated with this research are available and can be obtained by contacting the corresponding author.

APPENDIX A

JOHNSON MODEL

White (1975) assumes spherical gas patches much larger than the grains but much smaller than the wavelength. He developed the theory for a gas-filled sphere of porous medium of radius a located inside a water-filled sphere (brine here) of porous medium of outer radius b $(a < b)$. The saturation of gas is

$$S_g = \frac{a^3}{b^3}, \quad S_b = 1 - S_g. \tag{A-1}$$

White (1975) assumed that the dry-rock and grain moduli and permeability κ of the different regions are the same. For values of the gas saturation higher than 52%, or values of the brine saturation between 0% and 48%, the theory is not rigorously valid.

Johnson (2001) generalized White's theory to patches of arbitrary geometries, where "arbitrary" means that the patch shape is defined by the ratio surface of the patch to the total volume of the sample (for more details, see Tserkovnyak and Johnson, 2003). The dynamic bulk modulus $K(\omega)$ is consistent with the Gassmann-Wood (GW) modulus at low frequencies and to the Gassmann-Hill (GH) modulus at high frequencies. When the pore space is partially saturated with two very different fluids, such as gas and brine, a fast P-wave traveling in the medium induces very different pore pressures in the two regions, which tend to equilibrate through a diffusive phenomenon governed by the so-called Biot acoustic slow wave.

The effective P-wave bulk modulus of the two regions is

$$K_E = \frac{E_m M}{E_G} \tag{A-2}$$

(Carcione and Picotti, 2006), where

$$E_m = K_m + \frac{4}{3}\mu \tag{A-3}$$

is the dry-rock P-wave modulus, and

$$E_G = K_G + \frac{4}{3}\mu \tag{A-4}$$

(Carcione, 2014) is the P-wave wet-rock modulus, K_G is the Gassmann modulus (see below), K_m is the dry-rock bulk modulus, and μ is the dry-rock shear modulus. The fluid modulus M depends on the bulk modulus of the pore fluids K_i and is given by

$$M(K_i) = \left(\frac{\alpha - \phi}{K_s} + \frac{\phi}{K_i}\right)^{-1}, \quad i = g \text{ or } b, \tag{A-5}$$

where K_s is the solid-grain bulk modulus, and α (also known as the Biot-Willis coefficient) is defined as

$$\alpha = 1 - \frac{K_m}{K_s}. \tag{A-6}$$

The Gassmann bulk modulus for each fluid phase is given by

$$K_G = K_m + \alpha^2 M. \tag{A-7}$$

As shown by White (1975), slow-wave diffusion induces wave-velocity dispersion and attenuation of the fast P-wave, which depends mostly on the size of the gas pockets (saturation), frequency, permeability, and porosity of the rocks. At very low frequencies, there is enough time for pore pressure to equilibrate to a constant value. Therefore, the fluid pressure is uniform (isostress state), and the effective modulus of the pore fluid is given by Wood's modulus (e.g., Mavko et al., 2009), which is exact for the static modulus of two fluids:

$$K_f = \left(\frac{S_g}{K_g} + \frac{S_b}{K_b}\right)^{-1}, \tag{A-8}$$

In this case, the effective bulk modulus of the composite at the low frequency limit is given by the Gassmann expression

$$K_{GW} = K_m + \alpha^2 M(K_f) \tag{A-9}$$

and it is independent of the spatial distribution of the fluids. The process of equilibration is governed by the diffusion equation whose diffusivity constant is given by

$$D(K_i) = \frac{\kappa K_E}{\eta}, \quad i = g \text{ or } b, \tag{A-10}$$

where η is the viscosity of the respective fluid phase and the critical fluid diffusion relaxation length is given by $L_c = \sqrt{D/\omega}$.

In contrast, when the frequency is sufficiently high (e.g. smaller diffusion lengths) the pore pressures in the two phases do not have enough time to equilibrate within one half cycle. Consequently, the pressure is not uniform, but it can be assumed to be constant within each phase. In such a situation, the fluid flow effect can be ignored and Hill's theorem (Mavko et al., 2009) gives the composite bulk modulus at the high-frequency limit:

$$K_{GH} = \left(\frac{S_g}{E_{Gg}} + \frac{S_b}{E_{Gb}}\right)^{-1} - \frac{4}{3}\mu. \tag{A-11}$$

Pride et al. (1993) and Johnson (2001) propose the following expression for the complex bulk modulus:

$$K(\omega) = K_{GH} - \frac{K_{GH} - K_{GW}}{1 - \xi + \xi\sqrt{1 - i\omega\tau/\xi^2}}, \tag{A-12}$$

where

$$\tau = \left(\frac{K_{GH} - K_{GW}}{K_{GH}^2 \beta g}\right)^2, \qquad \xi = \frac{\beta g K_{GH}^2}{2K_{GW}T}\sqrt{\tau^3}, \tag{A-13}$$

$$g = \frac{\kappa}{\eta_g\sqrt{D_g} + \eta_b\sqrt{D_b}} \times \left[\frac{(R_b + Q_b)(K_{Gg} + 4\mu/3) - (R_g + Q_g)(K_{Gb} + 4\mu/3)}{\phi S_g K_{Gg}(K_{Gb} + 4\mu/3) + \phi S_b K_{Gb}(K_{Gg} + 4\mu/3)}\right]^2 \tag{A-14}$$

$$Q = \frac{(1 - \phi - K_m/K_s)\phi K_s}{1 - \phi - K_m/K_s + \phi K_s/K_i}, i = g \text{or} b, \tag{A-15}$$

$$R = \frac{\phi^2 K_s}{1 - \phi - K_m/K_s + \phi K_s/K_i}. \tag{A-16}$$

The parameter

$$\beta = S/V \tag{A-17}$$

depends on the shape of the patches, being the ratio of the surface area of a patch to the whole volume, whereas the parameter T is governed by the mean size of the patch, which can be solved only with certain simplifying geometries (Johnson, 2001). In the limit when one fluid phase is a vacuum, the parameter T is the mean time for diffusion across the fluid patch, or, in other words, the diffusion time for equilibrating stress in the porous skeleton over the size of a fluid patch. Tserkovnyak and Johnson (2002) show how to obtain β and T from experimental data.

Ellipsoidal patches

To illustrate a simple but more general case than a spherical patch, consider that the patch is a 3D ellipsoid with semiaxes a_j embedded in a sample ellipsoid of semiaxes b_j. The area of the inner ellipsoid is

$$S \approx 4\pi\left[\frac{(a_1a_2)^n + (a_1a_3)^n + (a_2a_3)^n}{3}\right]^{1/n}, \quad n = 1.6075, \tag{A-18}$$

whereas the volume of the outer ellipsoid is

$$V = \frac{4}{3}\pi b_1 b_2 b_3. \tag{A-19}$$

The parameter β, defined in equation A-17, is

$$\beta = 3^{(1-1/n)}\frac{[(a_1a_2)^n + (a_1a_3)^n + (a_2a_3)^n]^{1/n}}{b_1b_2b_3}. \tag{A-20}$$

For $a_1 = a_2 = a_3 = a$ and $b_1 = b_2 = b_3 = b$, we obtain equation A-25 below. The gas saturation is

$$S_g = \frac{a_1a_2a_3}{b_1b_2b_3}. \tag{A-21}$$

Assume that the outer ellipsoid is a uniform stretched version of the patch or inner ellipsoid, with stretching value $\gamma \geq 1$, such that $b_j = \gamma a_j$. Then

$$\beta = 3^{(1-1/n)}(a_1^{-n} + a_2^{-n} + a_3^{-n})^{1/n}S_g \tag{A-22}$$

since $S_g = \gamma^{-3}$.

Consider that $a_2 = a_1$ so that the ellipsoid becomes a spheroid. Then,

$$\beta = 3^{(1-1/n)}(2a_1^{-n} + a_3^{-n})^{1/n}S_g, n = 1.6075. \tag{A-23}$$

If $a_3 < a_1$, the ellipsoid is an oblate spheroid, and β is greater than that of a sphere with radius a_1, whereas if $a_3 > a_1$, the ellipsoid is a prolate spheroid, and β is smaller than that of a sphere with radius a_1. The spheroid can model penny-shaped patches if $a_1 \gg a_3$ and stick-shaped patches if $a_3 \gg a_1$. In contrast, parameter T for the spheroid requires a numerical calculation with equation 22 in Johnson (2001). The semiaxes a_1 and a_3 are both much smaller than the wavelength to satisfy the mesoscopic hypothesis. Assume $a_1 = 15$ cm and vary a_3 from 7.5 mm to 1.5 m, i.e., from an oblate to a prolate spheroid. β varies from 5.5/m to 3.1/m, with $\beta = 4/\text{m}$ for the sphere $(a_3 = a_1)$.

White model

Let us consider the concentric spherical geometry of White (1975). The two Johnson parameters have the following expression:

$$\beta = \frac{3a^2}{b^3} = \frac{3S_g}{a},$$
$$T = \frac{K_{GW}\phi^2}{30\kappa b^3}\{[3\eta_b s_b^2 + 5(\eta_g - \eta_b)s_g s_b - 3\eta_g s_g^2]a^5 - 15\eta_b s_b(s_b - s_g)a^3b^2 + 5s_b[3\eta_b s_b - (2\eta_g - \eta_b)s_g]a^2b^3 - 3\eta_b g_b^2 b^5\}, \tag{A-24}$$

where

$$s = \frac{(1 - K_m/K_s)(1/K_f - 1/K_i)}{1 - K_m/K_s - \phi K_m/K_s + \phi K_m/K_f}, \quad i = g \text{ or } b. \tag{A-25}$$

REFERENCES

Avseth, P., T. Mukerji, and G. Mavko, 2005, Quantitative seismic interpretation: Cambridge University Press.

Böhm, G., J. M. Carcione, D. Gei, S. Picotti, and A. Michelini, 2015, Cross-well electromagnetic and seismic tomography for CO_2 detection and monitoring in a saline aquifer: Journal of Petroleum Science and Engineering, **133**, 245–257, doi: 10.1016/j.petrol.2015.06.010.

Carcione, J. M., 2014, Wave fields in real media. Theory and numerical simulation of wave propagation in anisotropic, anelastic, porous and electromagnetic media, 3rd ed.: Elsevier.

Carcione, J. M., and P. Avseth, 2015, Rock-physics templates for clay-rich source rocks: Geophysics, **80**, no. 5, D481–D500, doi: 10.1190/geo2014-0510.1.

Carcione, J. M., D. Gei, S. Picotti, and A. Michelini, 2012, Cross-hole electromagnetic and seismic modeling for CO_2 detection and monitoring

in a saline aquifer: Journal of Petroleum Science and Engineering, **100**, 162–172, doi: 10.1016/j.petrol.2012.03.018.
Carcione, J. M., and S. Picotti, 2006, P-wave seismic attenuation by slow-wave diffusion: Effects of inhomogeneous rock properties: Geophysics, **71**, no. 3, O1–O8, doi: 10.1190/1.2194512.
Carcione, J. M., S. Picotti, D. Gei, and G. Rossi, 2006, Physics and seismic modeling for monitoring CO_2 storage: Pure and Applied Geophysics, **163**, 175–207, doi: 10.1007/s00024-005-0002-1.
Carman, P. C., 1961, L' écoulement des gaz á travers les milieux poreux, Bibliothéque des Sciences et Techniques Nucléaires: Presses Universitaires de France.
Engelsen, C. W. D., J. C. Isarin, H. Gooijer, M. M. C. G. Warmoeskerken, and J. G. G. Wassink, 2002, Bubble size distribution of foam: Autex Research Journal, **2**, 14–27.
Dvorkin, J., and G. Mavko, 2006, Modeling attenuation in reservoir and nonreservoir rock: The Leading Edge, **25**, 194–916, doi: 10.1190/1.2172312.
Hamby, D. M., 1994, A review of techniques for parameter sensitivity analysis of environmental models: Environmental Monitoring Assessment, **32**, 135–154, doi: 10.1007/BF00547132.
Hashin, Z., and S. Shtrikman, 1963, A variational approach to the theory of the elastic behavior of multiphase materials: Journal of Mechanics and Physics of Solids, **11**, 127–140, doi: 10.1016/0022-5096(63)90060-7.
Herron, M. M., 1987, Estimating the intrinsic permeability of clastic sediments from geochemical data: Transactions of the SPWLA 28 the Annual Logging Symposium (paper HH), London, UK.
Johnson, D. L., 2001, Theory of frequency dependent acoustics in patchy-saturated porous media: Journal of the Acoustical Society of America, **110**, 682–694, doi: 10.1121/1.1381021.
Krief, M., J. Garat, J. Stellingwerff, and J. Ventre, 1990, A petrophysical interpretation using the velocities of P and S waves (full waveform sonic): The Log Analyst, **31**, 355–369.
Man, C.-S., and M. Huang, 2011, A simple explicit formula for the Voigt-Reuss-Hill average of elastic polycrystals with arbitrary crystal and texture symmetries: Journal of Elasticity, **105**, 29–48, doi: 10.1007/s10659-011-9312-y.
Mavko, G., T. Mukerji, and J. Dvorkin, 2009, The rock physics handbook: Tools for seismic analysis in porous media: Cambridge University Press.
Müller, T. M., B. Gurevich, and M. Lebedev, 2010, Seismic wave attenuation and dispersion resulting from wave-induced flow in porous rocks — A review: Geophysics, **75**, no. 5, A147–A164.
Müller, T. M., J. Toms-Stewart, and F. Wenzlau, 2008, Velocity-saturation relation for partially saturated rocks with fractal pore fluid distribution: Geophysical Research Letters, **35**, L09306, doi: 10.1029/2007GL033074.
Picotti, S., J. M. Carcione, D. Gei, G. Rossi, and J. E. Santos, 2012, Seismic modeling to monitor CO_2 geological storage: The Atzbach-Schwanenstadt gas field: Journal of Geophysical Research: Solid Earth, **117**, B06103, doi: 10.1029/2011JB008540.
Picotti, S., J. M. Carcione, G. Rubino, J. E. Santos, and F. Cavallini, 2010, A viscoelastic representation of wave attenuation in porous media: Computer & Geosciences, **36**, 44–53, doi: 10.1016/j.cageo.2009.07.003.
Picotti, S., and J. M. Carcione, 2017, Numerical simulation of wave-induced fluid flow seismic attenuation based on the Cole-Cole model: Journal of the Acoustical Society of America, **142**, 134, doi: 10.1121/1.4990965.
Pride, S. R., F. D. Morgan, and A. F. Gangi, 1993, Drag forces of porous-medium acoustics: Physical Review B, **47**, 4964–4978, doi: 10.1103/PhysRevB.47.4964.
Tiab, D., and E. C. Donaldson, 2015, Petrophysics: Theory and practice of measuring reservoir rock and fluid transport properties, 4th ed.: Gulf Professional Publishing.
Toms, J., T. M. Müller, and B. Gurevich, 2007, Seismic attenuation in porous rocks with random patchy saturation: Geophysical Prospecting, **55**, 671–678, doi: 10.1111/j.1365-2478.2007.00644.x.
Tserkovnyak, Y., and D. L. Johnson, 2002, Can one hear the shape of a saturation patch?: Geophysical Research Letters, **29**, 12, doi: 10.1029/2001GL014709.
Tserkovnyak, Y., and D. L. Johnson, 2003, Capillary forces in the acoustics of patchy-saturated porous media: Journal of the Acoustical Society of America, **114**, 2596–2606.
White, J. E., 1975, Computed seismic speeds and attenuation in rocks with partial gas saturation: Geophysics, **40**, 224–232, doi: 10.1190/1.1440520.